Proc. Natl. Acad. Sci. USA
Vol. 92, pp. 5577–5581, June 1995
Neurobiology

Emergent spindle oscillations and intermittent burst firing in a thalamic model: Specific neuronal mechanisms

(thalamus/nucleus reticularis thalami/biophysical network modeling/synchrony)

X.-J. WANG*, D. GOLOMB†, AND J. RINZEL†

*Department of Mathematics, University of Pittsburgh, Pittsburgh, PA 15260; and †Mathematical Research Branch, National Institute of Diabetes and Digestive and Kidney Diseases, National Institutes of Health, 9190 Wisconsin Avenue, Suite 350, Bethesda, MD 20814

Communicated by Per Andersen, University of Oslo, Oslo, Norway, February 17, 1995 (received for review October 5, 1994)

ABSTRACT **The rhythmogenesis of 10-Hz sleep spindles is studied in a large-scale thalamic network model with two cell populations: the excitatory thalamocortical (TC) relay neurons and the inhibitory nucleus reticularis thalami (RE) neurons. Spindle-like bursting oscillations emerge naturally from reciprocal interactions between TC and RE neurons. We find that the network oscillations can be synchronized coherently, even though the RE–TC connections are random and sparse, and even though individual neurons fire rebound bursts intermittently in time. When the fast γ-aminobutyrate type A synaptic inhibition is blocked, synchronous slow oscillations resembling absence seizures are observed. Near-maximal network synchrony is established with even modest convergence in the RE-to-TC projection (as few as 5–10 RE inputs per TC cell suffice). The hyperpolarization-activated cation current (I_h) is found to provide a cellular basis for the intermittency of rebound bursting that is commonly observed in TC neurons during spindles. Such synchronous oscillations with intermittency can be maintained only with a significant degree of convergence for the TC-to-RE projection.**

The 7- to 14-Hz spindle oscillation, which concurs with the onset of sleep, is a well-known phenomenon of coherent brain waves. Its thalamic origin was demonstrated 50 years ago (1). Since then spindle rhythmicity in thalamocortical (TC) relay neurons has been shown to result from the integrative effects of synaptic inhibition with special intrinsic membrane properties of these cells (2–4). The critical role of the nucleus reticularis thalami (RE) was suggested by the Scheibels (5) and has been established by the work of Steriade *et al.* (3, 4). γ-Aminobutyratergic (GABAergic) neurons in the RE produce inhibitory postsynaptic potentials (IPSPs) in TC neurons, leading to rebound bursts of spikes, which in turn excite RE neurons. The rebound response to IPSPs is produced by a low-threshold T-type Ca^{2+} current (I_T) (6, 7) and a hyperpolarization-activated cation current (I_h) (8, 9) in TC cells.

Recent experiments have crystalized some of the critical issues concerning spindle rhythmogenesis, which are not yet fully understood. For instance, regarding the intrathalamic circuit bases of spindling, an *in vivo* experiment on the cat showed that an isolated RE network is capable of displaying coherent spindle oscillations (10), probably due to intra-RE recurrent inhibitory connections (3, 4, 11–13). The spindle wave activity, however, can also result from the two-way RE–TC interactions (3, 14). More recently, *in vitro* spontaneous spindling has been demonstrated in a ferret thalamic slice preparation (15, 16): (*i*) during spontaneous spindles RE cells fired bursts almost at the population rhythmic frequency (about 6 Hz) but occasionally skipped cycles, whereas TC cells fired bursts at half of that rate or lower; (*ii*) with the application of $GABA_A$ receptor antagonists, RE and TC cells fired bursts very regularly at about 3 Hz; (*iii*) with $GABA_B$ receptor antagonists, no significant change was noticed; (*iv*) when both the $GABA_A$ and $GABA_B$ synaptic inhibitions were blocked; or (*v*) when the α-amino-3-hydroxy-5-methyl-4-isoxazolepropionate (AMPA) synaptic excitation was blocked, the network was quiescent. Therefore, the spindle oscillations observed in ferret thalamic slices depended critically on the reciprocal connections between the TC and RE cell types.

Here, we study a thalamic network model consisting of a large population of TC neurons that interact reciprocally with a large population of RE neurons. This allows us to investigate the following basic issues on thalamic spindles which could not have been adequately addressed in previous modeling works, when only a single representative TC cell was included (12, 17). First, we seek here to reproduce the *in vitro* results (*i–v*) of McCormick and colleagues (15, 16) and to shed light on their underlying cellular and synaptic mechanisms. Second, since quantitative anatomical data on the intrathalamic circuit remain scarce at the present time, we use a computational approach to assess properties of the RE–TC reciprocal connections, especially their divergence/convergence factors, that are required for generating a high degree of coherence during spindles. Third, we are concerned with the common observation that spindling TC cells fire rebound bursts only once in several rhythmic cycles (2, 4, 7, 14–16), and we explain this intermittency phenomenon in terms of a temporal integration of synaptic inhibition by the intrinsic slow inward current I_h of TC cells, as proposed by Kopell and LeMasson (18) as well as by us (ref. 19; X.-J.W. and J.R., unpublished work).

NETWORK MODEL

Biophysical models of single RE and TC neurons were reported elsewhere (12). The single-compartment model neurons contain only ionic currents that have been shown experimentally to play a crucial role in the low-threshold spikes of spindle oscillations. For the sake of simplicity, the Na^+ spike-generating currents (20) are not included. A RE neuron has an I_T; a Ca^{2+}-activated, voltage-independent ("after-hyperpolarization") K^+ current (I_{AHP}); and a leak current. A TC neuron possesses an I_T, an I_h, and a leak current. The leak current is decomposed into two components, a nonspecific component [$I_L = g_L(V - V_L)$] and a K^+ component [$I_{KL} = g_{KL}(V - V_K)$]. The K^+ leak conductance (g_{KL}) is considered as a "sleep parameter" in the model, since it has been shown that the slow sleep rhythms in the thalamic circuit are conditioned by neuromodulators which act on TC and RE cells largely by varying a g_{KL} (21). The standard parameter values for single neurons are as follows. For RE neurons; $g_T = 1.5$, $g_{AHP} = 0.1$, $g_L = 0.04$, and $g_{KL} = 0.02$ (mS/cm^2); $V_L = -82.5$ and $V_{KL} = -90$ (mV). For TC neurons, $g_T = 2$, $g_h = 0.04$, $g_L = 0.01$, and

The publication costs of this article were defrayed in part by page charge payment. This article must therefore be hereby marked "*advertisement*" in accordance with 18 U.S.C. §1734 solely to indicate this fact.

Abbreviations: AMPA, α-amino-3-hydroxy-5-methyl-4-isoxazolepropionate; GABA, γ-aminobutyrate; IPSP, inhibitory postsynaptic potential; RE, nucleus reticularis thalami; TC, thalamocortical.

g_{KL} = 0.02 (mS/cm^2); V_L = −70 and V_{KL} = −100 (mV). Neurons of each cell type are identical and deterministic.

The network model consists of N_{RE} RE neurons and N_{TC} TC neurons coupled by reciprocal connections; intra-RE connections are also included. The circuit connectivity is assumed to be random. Consider for instance the RE inputs to TC neurons. Each RE cell sends its output to a given TC cell with probability p_{RT}; hence on average there are $M_{RT} = p_{RT}N_{RE}$ RE inputs per TC cell. [M_{RT} is the convergence factor for the RE-to-TC projection; the divergence factor is $M_{RT}(N_{TC}/N_{RE})$.] Similar random connectivity is assigned to the TC-to-RE projection and the RE-to-RE lateral projection, with M_{TR} and M_{RR} mean inputs per RE neuron, respectively. There is no coupling among TC cells. Accurate experimental estimates for the ratio N_{RE}/N_{TC} and connectivity parameters M_{RT}, M_{TR}, and M_{RR} are presently not available. In simulations we set $N_{RE} = N_{TC} = 1000$, and our results are expected to be valid in the limit of large networks. Typically, a sparse connectivity is prescribed, with $M_{RT} = M_{TR} = M_{RR} = 10$ (so that, for example, $p_{RT} = M_{RT}/N_{RE} = 0.01$). For comparison, we also considered the all-to-all coupling limit ($M_{RT} = M_{RR} = N_{RE}$, $M_{TR} = N_{TC}$).

The TC-to-RE excitation is assumed to be mediated by fast glutamate synapses of the AMPA subtype. The RE-to-TC inhibition has two components, mediated by fast $GABA_A$ and slow $GABA_B$ synapses. Only $GABA_A$ interactions are included for mutual inhibition within the RE circuit. The AMPA and $GABA_A$ synaptic currents are modeled according to refs. 11 and 12. The $GABA_B$ synaptic current, known to be activated through a heterotrimeric guanine nucleotide-binding protein (G protein), is modeled by a simple scheme with two first-order kinetic steps. Assume that $I_{GABA\text{-}B} = g_{GABA\text{-}B}s^q(V - V_K)$, where s is a gating variable and $q = 4$. Then, $dx/dt = \alpha_x X(V_{pre})(1 - x) - \beta_x x$, and $ds/dt = \alpha_s x(1 - s) - \beta_s s$. In these equations, x represents concentration of a dissociated G-protein subunit. The concentration of the postsynaptic transmitter–receptor complex, $X(V)$, is assumed to be an instantaneous and sigmoid function of the presynaptic membrane potential, $X(V) = \{1 + \exp[-(V + 45)/2]\}^{-1}$, −45 mV being a presumed threshold for the transmitter release. The parameters $\alpha_x = 5.0$, $\beta_x = 0.007$, $\alpha_s = 0.03$, and $\beta_s = 0.005$ (ms^{-1}) were chosen so that the rise time (≈100 ms) and the decay time (≈200 ms) of the $GABA_B$ synaptic current elicited by a brief presynaptic pulse are matched with the experimental measurements (22, 23).

The standard synaptic parameter values are as follows (maximal conductances in mS/cm^2, voltage in mV). For RE-to-TC synapses, $g_{GABA\text{-}A} = 0.2$, $g_{GABA\text{-}B} = 0.02$, $V_{GABA\text{-}A} = -85$, and $V_{GABA\text{-}B} = -100$. For RE-to-RE synapses, $g_{GABA\text{-}A} = 0.2$ and $V_{GABA\text{-}A} = -75$. For TC-to-RE synapses, $g_{AMPA} = 0.08$ and $V_{AMPA} = 0$. The maximal conductances are normalized by the mean number of synaptic inputs, M, so that when the convergence factor M is varied, the average total synaptic drive per cell remains the same. This is necessary especially in the all-to-all coupling case, where M is proportional to the network size and can be very large.

Numerical integration was carried out with the fourth-order Runge–Kutta method, typically with a time step of 0.5 ms. As initial conditions, the membrane potentials are randomly distributed between −80 and −70 mV, and the current gating variables are at their corresponding steady-state values. The global network behavior is characterized by two types of quantities: the fraction of cells that are simultaneously active (above the synaptic threshold of −45 mV), $\rho_{RE}(t)$ and $\rho_{TC}(t)$, and the population-averaged membrane potentials, $\bar{V}_{RE}(t)$ and $\bar{V}_{TC}(t)$. The coherence of network oscillations is measured by the normalized temporal variances of $\bar{V}_{RE}(t)$ and $\bar{V}_{TC}(t)$, which are denoted by χ_{RE} and χ_{TC}, respectively (see refs. 12, 24, and 25).

RESULTS

Dependence of Spindle Oscillations on Reciprocal RE–TC Connections. The thalamic network model as specified above displays coherent oscillations at about 7.7 Hz (Fig. 1*A*). The TC cell population dynamically segregates approximately into two firing clusters that fire rebound bursts alternately in time, at half of the network frequency [as seen in $\rho_{TC}(t)$]. Individual RE neurons typically receive inputs from both TC clusters and are thereby excited to fire a burst at about every cycle.

To assess the connectivity dependence of the rhythm, $GABA_A$ synaptic transmission is first blocked (Fig. 1*B*), mimicking the experiment with bicuculline (15, 16). Both RE and TC cells display powerful bursting oscillations (at 3.4 Hz) that are perfectly synchronized. This behavior is similar to that seen by McCormick and colleagues (15, 16) and reminiscent of that observed during absence seizures (26). Note that the burst duration in RE cells is about twice as large as in the "intact" case (compare Fig. 1 *A* and *B*), in agreement with the experimental observations (15, 16). In the present model this duration increase is largely due to the loss of intra-RE $GABA_A$ inhibition that normally cuts short the burst. With different initial conditions we observed two other types of behaviors that coexist with this synchronous slow oscillation. One is the rest state (where the network is quiescent). In the other, TC cells fire bursts repetitively at 3 Hz but are no longer synchronized (data not shown). In this case, RE cells fire at higher rates (>5 Hz); the slowly decaying $GABA_B$ synaptic inhibition yields a nearly constant hyperpolarization and does not provide phasic information to synchronize the TC cells. A decrease of the excitatory TC-to-RE synaptic conductance (g_{AMPA}), which decreases the RE firing rate, eliminated this asynchronous state.

If both the $GABA_A$ and $GABA_B$ synapses are blocked, or if only the AMPA synapses are blocked, the network becomes silent (data not shown). In the disconnected network, the resting membrane potential is −63 mV for TC neurons and −84 mV for RE neurons. Hence, as in the *in vitro* ferret slice experience (15, 16), the RE–TC interactions in both directions are needed for achieving coherent network rhythmicity in our model. Oscillations emerge in a self-consistent fashion: the

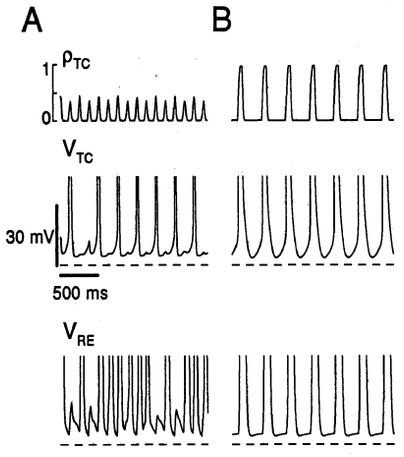

FIG. 1. (*A*) Rhythmic burst oscillations of the thalamic network model; population frequency f = 7.7 Hz. A RE neuron (*Bottom*) fires bursts at about twice the frequency of a TC neuron (*Middle*) (the membrane potential is clipped at −45 mV; dashed baseline is at −90 mV). The bursts have large amplitudes, because several voltage-dependent K^+ currents were not included in our model neurons. The TC cell population segregates approximately into two clusters that fire rebound bursts alternately in time. For this periodic TC population activity (*Top*), $\rho_{TC}(t)$ (the fraction of TC cells that are suprathreshold) shows a maximum amplitude of about 50%. (*B*) When $GABA_A$ synapses are blocked, the entire network oscillates at 3.4 Hz, in perfect synchrony. Note the enlargement of burst width in both TC and RE neurons, due to the lack of fast $GABA_A$ inhibition.

resting membrane potential of RE neurons is sufficiently hyperpolarized so that transient depolarizing input from TC neurons can produce powerful burst responses in RE neurons, which in turn provide synaptic inhibition and elicit rebound bursts in TC neurons (27).

Under suitable parameter changes, single RE or TC neurons may become intrinsic oscillators. In that case, blocking synapses would only disrupt synchrony but would not abolish cellular oscillations (data not shown).

The RE-to-TC Convergence and Spindle Synchrony. As the RE-to-TC convergence factor M_{RT} is varied systematically, the coherence measure χ_{TC} displays a quite nonlinear dependence (Fig. 2). When M_{RT} is below a critical value the network is virtually completely asynchronous; hence, χ_{TC} is almost zero (and this residual value decreases with increasing network size). Above the well-defined transition value of M_{RT}, χ_{TC} reaches a large value (0.5–0.6) and saturates (Fig. 2, solid curve). The quantity χ_{TC} does not approach the value of 1, since, in this regime, the TC cell population is not fully synchronized but breaks itself into two clusters. When the intra-RE connections are blocked, the synchronous behavior occurs at even smaller values of M_{RT} (Fig. 2, dashed curve). This is due to the combined effects of the reciprocal $GABA_A$ fast inhibition between RE cells: it reduces the IPSP amplitudes in the TC cells that promote the network synchronization (15, 16, 27); and it tends to dynamically fracture the RE network into mutually out-of-phase clusters (11–13, 24, 25). A similar asynchrony-to-synchrony transition was also found when the convergence factor M_{TR} for the TC-to-RE projection was varied (data not shown).

Intermittent Bursting in TC Neurons. The TC neurons generally fire rebound bursts at a rate lower than the network rhythmic frequency. To quantify this phenomenon, we computed first the power spectrum of the global variable $\rho_{RE}(t)$ or $\rho_{TC}(t)$ and identified the frequency f at maximum power as the population rhythmic frequency. Then, the bursting rate for each of the TC neurons was computed and averaged over the entire TC population, yielding the mean TC bursting rate, $\langle f \rangle_{TC}$. The bursting ratio $k_{TC} = f/\langle f \rangle_{TC}$ measures the degree of intermittency of spindling TC cells. Note that f and k_{TC} can vary with the realization of the connectivity pattern and with initial conditions.

TC firing becomes more intermittent (k_{TC} larger) with increased hyperpolarization, for instance when the K^+ leak conductance is increased. In Fig. 3, with $g_{KL} = 0.04$ mS/cm^2 for TC cells (as compared to Fig. 1 with $g_{KL} = 0.02$ mS/cm^2), the network frequency drops to $f = 6.3$ Hz; the period $T_p = 1/f \simeq 157$ ms. The TC network now segregates into more than two approximate clusters. The bursts of individual TC cells are always phase-locked with the population rhythm but are not necessarily synchronized with each other. Hence, at each network cycle only a small fraction (at most 20–25%) of the TC population fire bursts almost simultaneously [see $\rho_{TC}(t)$ in Fig. 3*A*]. The intermittent firing pattern is further illustrated by the

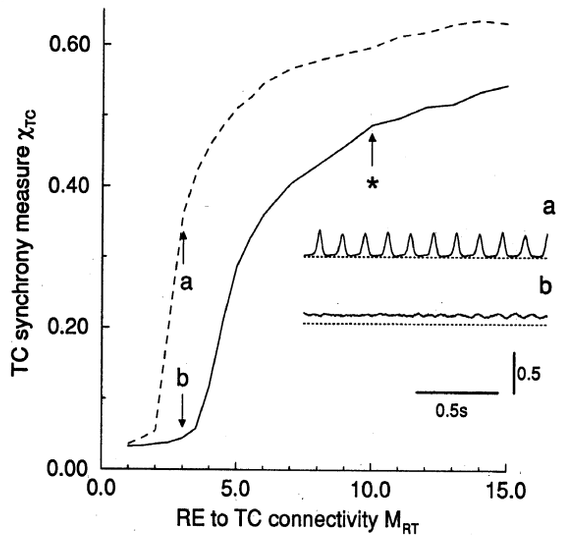

FIG. 2. Dependence of the TC synchrony measure χ_{TC} on the RE-to-TC convergence factor M_{RT} with (solid line) or without (dashed line) intra-RE $GABA_A$ inhibition. There is a sharp but continuous transition from an asynchronous state at low M_{RT} to a synchronized state at higher M_{RT} values. The quantity χ_{TC} was computed by averaging over a time interval of 10 sec and over five realizations of connectivity patterns and initial conditions, for each parameter value. (*Inset*) Time courses of population activity $\rho_{TC}(t)$ for $M_{RT} = 4$ with (curve a) and without (curve b) intra-RE inhibition (scales apply to both). Dotted line denotes the zero level. Asterisk at $M_{RT} = 10$ corresponds to Fig. 1*A*. $M_{TR} = M_{RR} = 10$.

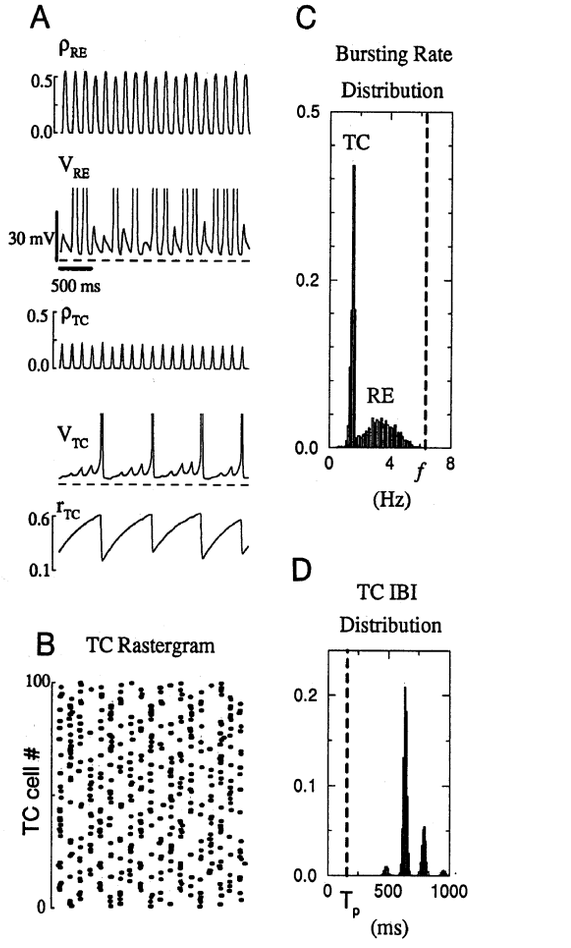

FIG. 3. Intermittent burst firing during spindles (same parameters as in Fig. 1, except $g_{KL} = 0.04$ instead of 0.02 mS/cm^2 for TC cells); the population frequency is 6.3 Hz. (*A*) Population activities, ρ_{RE} and ρ_{TC}, are rhythmic and quite regular. At each network cycle <25% of TC neurons fire bursts simultaneously. As illustrated by two membrane potential time courses (the membrane potential is clipped at −45 mV; dashed baseline: −90 mV), RE cells occasionally skip a network rhythmic cycle, while TC cells fire rebound bursts once in three to five cycles. A TC cell's I_h slowly accumulates during subthreshold cycles and de-activates quickly during a rebound burst (as shown by its gating variable r_{TC}). (*B*) The intermittent firing patterns are also seen in the rastergram of 100 TC neurons. (The time scale applies to all panels in *A* and *B*.) (*C*) The normalized histogram of TC and RE cells' time-averaged bursting rates (bin = 0.1 Hz). TC neurons fire at a lower rate than RE neurons, both below the network rhythmic frequency ($f = 6.3$ Hz, dashed vertical line). The histograms were obtained by computing the mean bursting rates of all cells averaged over a time interval of 10 s. (*D*) Normalized interburst interval (IBI) histogram (bin = 10 ms) calculated for all IBIs from the entire TC population (dashed vertical line: the population oscillation period, $T_p = 157$ ms). In *C* and *D*, the distributions were normalized by dividing the number of events within each bin by the total number of events.

rastergram (Fig. 3*B*) of 10% of the TC neurons (100 out of the total 1000). The RE neurons do not fire at every cycle either; instead they fire quite irregularly, and often skip rhythmic cycles (Fig. 3*A*). This is because the excitatory inputs to each RE cell fluctuate considerably: they come from a limited number of TC cells (with the average $M_{TR} = 10$), and only a small fraction of them fire at each cycle due to the intermittency effect. For the same reasons, the overall excitation by TC inputs varies considerably from one RE cell to another, and RE cells display different mean bursting rates.

The intermittent firing of TC neurons is critically dependent on their intrinsic cellular properties, especially on I_h (19). The activation of I_h is voltage dependent, requires sufficient hyperpolarization, and is fairly slow (maximal time constant ≈ 1 s). By contrast, its deactivation at depolarized voltage levels is very fast. Therefore, as is shown in Fig. 3*A*, during a strong rebound burst, the activation gating variable (r_{TC}) of I_h quickly drops to a very small value, and I_h becomes negligible. Without I_h a TC cell would be too deeply hyperpolarized to generate postinhibitory rebound bursts. After a burst, a TC cell remains subthreshold for several cycles, while r_{TC} gradually accumulates until I_h reaches a critical value, and the cell fires a full rebound burst at the next cycle.

Fig. 3*C* shows the bursting rate distributions for the RE and TC populations. As expected, the TC distribution peaks at a lower frequency (about 1.6 Hz) than the RE distribution (about 3.5 Hz), both below the network rhythmic frequency (6.3 Hz). The RE distribution is significantly more dispersed than the TC distribution, reflecting the fact that TC inputs to RE neurons are quite variable in the intermittent bursting regime. The distribution of TC interburst intervals was computed for the entire TC population (Fig. 3*D*). The maximum is located at about $4T_p$, although peaks of large amplitudes are seen at $3T_p$ and $5T_p$. Small peaks exist at $2T_p$ (not visible) and $6T_p$. Therefore, TC neurons fire rebound bursts once in every two to six cycles, with the intermittency measure $k_{TC} \approx 4.3$.

The dependence of the degree of intermittency on the hyperpolarization level of TC cells is further quantified in Fig. 4*A*. Thus, k_{TC} increases as g_{KL} is strengthened. Since the population oscillation frequency f decreases (e.g., $f = 7.7$ Hz in Fig. 1 and 6.3 Hz in Fig. 3), and since $k_{TC} = f/\langle f \rangle_{TC}$, we see that the TC bursting rate $\langle f \rangle_{TC}$ drops even faster than f does. When g_{KL} is too large (above a critical value of about 0.047 mS/cm^2), TC neurons are completely hyperpolarized and the entire RE–TC network becomes quiescent. A similar increase of k_{TC} is observed when g_h is diminished (Fig. 4*B*), demonstrating the strong dependence of the phenomenon on g_h. To confirm that intermittency is essentially a dynamical phenomenon and depends less on the randomness of sparse connectivity, we performed the same computations with all-to-all connectivity (Fig. 4, dashed curves). In the latter case, the TC cells usually segregate into clusters that burst alternately, whereas the RE cells burst together at every cycle. As g_{KL} and g_h is varied, k_{TC} varies by discontinuous steps from one integer to another (Fig. 4). Comparing the results for all-to-all and sparse coupling, one sees that the randomness of connectivity smooths the dependence of k_{TC} on the parameters, and k_{TC} changes more dramatically with sparse connectivity than with all-to-all connectivity.

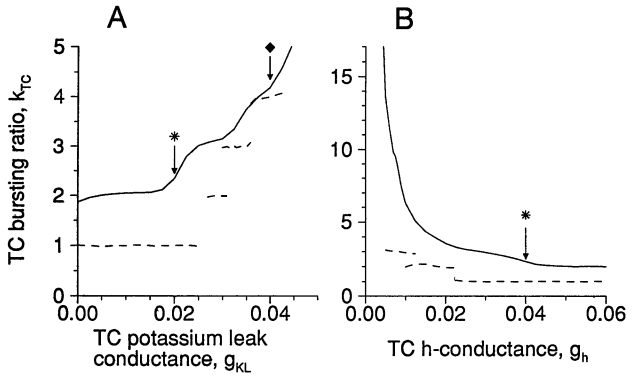

FIG. 4. Dependence of the TC bursting ratio (k_{TC}) on the K^+ leak conductance (g_{KL}) (*A*) and g_h (*B*) in TC cells: Comparison for sparse coupling ($M_{RT} = M_{TR} = M_{RR} = 10$, solid lines) and for all-to-all coupling (dashed line). The bursting ratio increases with g_{KL} as the TC cells become more hyperpolarized. Distinct regimes are observed for all-to-all coupling; sparseness smooths the transitions. With sparse coupling, the bursting ratio becomes large at small g_h values, as many neurons are quiescent and the remaining ones burst at low rates. The k_{TC} value was computed by averaging over a time interval of 10 s and over five realizations of connectivity patterns and initial conditions, for each parameter value. The asterisks correspond to the parameter set of Fig. 1*A*, and the diamonds to that of Fig. 3.

DISCUSSION

Since the pioneering work of Andersen and Andersson (2), the rhythmogenesis of thalamic spindles has been hypothesized to arise from divergent projections from inhibitory neurons which simultaneously hyperpolarize many TC neurons and induce subsequent rebound bursts in these cells. Here we have presented a large-scale thalamic network model and shown that coherent oscillations can emerge by this mechanism as a collective phenomenon, even when no single neuron is an intrinsic oscillator (Fig. 1). We have quantitatively assessed the properties of the RE–TC connections that are necessary for spindle rhythmogenesis, and revealed a transition from asynchrony to synchrony as the convergence/divergence factors of connectivity were varied (Fig. 2). Interestingly, global network synchrony can be realized even with a small value of 5–10 RE-to-TC convergence factor (see also ref. 28). Moreover, we predict that the blockade of intra-RE fast inhibitory synapses generally enhances the global synchrony of the thalamic network (Fig. 2). This is supported by the observation that an enhancement of intra-RE $GABA_A$ synapses, the mechanism by which the antiseizure drug clonazepam (27) may act, interferes with synchronized rhythmogenesis in the thalamus. We conclude that the synchronization of 10-Hz spindle oscillations can be robustly realized by the RE–TC reciprocal interactions, with reasonable and minimal assumptions about the underlying synaptic circuitry. To model and analyze other aspects of the network behaviors, however, more quantitative descriptions about the intrathalamic network architecture are highly desirable.

The present modeling was partly motivated by the *in vitro* experiments of McCormick and colleagues (15, 16). Our computer simulations reproduced many of their main observations, indeed all (*i–v*) as enumerated in the Introduction. In particular, a transition from an 8-Hz spindle-like oscillation to a 3-Hz absence seizure-like oscillation was demonstrated when the fast $GABA_A$ synapses were blocked (Fig. 1). However, we found that this latter result is in fact somewhat fragile, in the following sense. On one hand, during the 8-Hz spindle-like network activity, RE cells fire close to the population rhythmic frequency (15, 16). To reproduce this characteristic, relatively strong g_{AMPA} is needed to ensure that RE cells are sufficiently excited by a small number of intermittently firing TC cells. On the other hand, with the $GABA_A$ blockade, the network is desynchronized for large g_{AMPA} values (say >0.1 mS/cm^2) when the bursting rates of RE cells are sufficiently high (see *Results*). To compromise, we used intermediate g_{AMPA} values, in which case the synchronous state typically coexists with the asynchronous one, either of the two being observable with different initial conditions. This was not reported by McCormick and colleagues (15, 16) and may indicate certain deficiencies of our model. The model may be improved in the future on the basis of further biological constraints.

During spindles, the thalamic network as monitored by population-averaged quantities displays remarkably regular oscillations, whereas single neurons fire rebound bursts fairly intermittently, but always phase-locked to the population rhythm (2, 4, 7, 14–16). Theoretical studies of a single TC neuron (ref. 19; X.-J.W. and J.R., unpublished work) and of a large-scale thalamic network model (Figs. 3 and 4) clearly demonstrate that intermittent burst firing in TC neurons can be explained in terms of a temporal integration of rhythmic IPSPs by the current I_h (see also refs. 18 and 29). However, the I_h-dependent intermittent firing occurs only if the gating kinetics of I_h are significantly, but not too much, slower than the rhythmicity in question (19). If RE cells are not intrinsic oscillators, the intermittent network oscillation also depends on the circuit properties—i.e., RE cells should receive adequate convergent synaptic excitation from TC cells for most of the rhythmic cycles. As we demonstrated with all-to-all coupling, and in contrast with the work of Kopell and LeMasson (18), our model's TC cells segregate spontaneously into firing clusters, without heterogeneity, noise, or sparseness. On the other hand, the experimental observation that RE cells occasionally skip bursts could not be reproduced with all-to-all coupling in our simulations, even in the presence of strong neuroelectric noise (data not shown). With sparse connectivity, skipping can occur, since each RE cell now receives inputs from a limited number of intermittently bursting TC cells and sometimes is not sufficiently excited to reach the firing threshold. The dependence of intermittent bursting on I_h may be testable experimentally—for instance, by use of pharmacological blockers of g_h. In the thalamus, the degree of intermittency of TC cells' firing can be controlled by modulatory transmitters such as norepinephrine and serotonin, which act on TC neurons by varying a K^+ leak conductance, or by modulating the activation kinetics of g_h (21).

To conclude, some of our results may be relevant to other brain rhythms in the central nervous system (for a recent review, see ref. 30). First, we have shown how network oscillations may arise from a circuit based on synaptic inhibition and rebound excitation, rather than recurrent synaptic excitation. Second, we have demonstrated that a high degree of network synchronization may be realized even with random and very sparse connectivities. Third, intermittent firing of single cells may result from an integration of synaptic inputs by a slow intrinsic membrane process.

We thank D. A. McCormick for discussions. X.-J.W. was supported by the National Science Foundation (Grant IBN-9409202) and by an Alfred P. Sloan Fellowship. Some simulations were carried out at the National Cancer Institute Biomedical Supercomputing Center.

1. Morison, R. S. & Bassett, D. L. (1945) *J. Neurophysiol.* **8,** 309–314.
2. Andersen, P. & Andersson, S. A. (1968) *Physiological Basis of the Alpha Rhythm* (Appleton–Century–Crofts, New York).
3. Steriade, M. & Deschênes, M. (1984) *Brain Res. Rev.* **8,** 1–63.
4. Steriade, M., Jones, E. G. & Llinás, R. R. (1990) *Thalamic Oscillations and Signaling* (Wiley, New York).
5. Scheibel, M. E. & Scheibel, A. B. (1967) *Brain Res.* **6,** 60–94.
6. Jahnsen, H. & Llinás, R. R. (1984) *J. Physiol. (London)* **349,** 205–247.
7. Deschênes, M., Paradis, M., Roy, J. P. & Steriade, M. (1984) *J. Neurophysiol.* **51,** 1196–1219.
8. McCormick, D. A. & Pape, H.-C. (1990) *J. Physiol. (London)* **431,** 291–318.
9. Leresche, N., Lightowler, S., Soltesz, I., Jassik-Gerschenfeld, D. & Crunelli, V. (1991) *J. Physiol. (London)* **441,** 155–174.
10. Steriade, M., Domich, L., Oakson, G. & Deschênes, M. (1987) *J. Neurophysiol.* **57,** 260–273.
11. Wang, X.-J. & Rinzel, J. (1993) *Neuroscience* **53,** 899–904.
12. Golomb, D., Wang, X.-J. & Rinzel, J. (1994) *J. Neurophysiol.* **72,** 1109–1126.
13. Destexhe, A., Contreras, D., Sejnowski, T. & Steriade, M. (1994) *J. Neurophysiol.* **72,** 803–818.
14. Buzsáki, G. (1991) *Neuroscience* **41,** 351–364.
15. von Krosigk, M., Bal, T. & McCormick, D. A. (1993) *Science* **261,** 361–364.
16. Bal, T., von Krosigk, M. & McCormick, D. A. (1994) *J. Physiol. (London)* **483,** 641–663, 665–685.
17. Destexhe, A., McCormick, D. A. & Sejnowski, T. J. (1993) *Biophys. J.* **65,** 2473–2477.
18. Kopell, N. & LeMasson, G. (1994) *Proc. Natl. Acad. Sci. USA* **91,** 10586–10590.
19. Wang, X.-J. (1994) *Neuroscience* **59,** 21–31.
20. Huguenard, J. R. & McCormick, D. A. (1992) *J. Neurophysiol.* **68,** 1373–1383.
21. McCormick, D. A. (1992) *Prog. Neurobiol.* **39,** 337–388.
22. Otis, T. S., De Konink, Y. D. & Mody, I. (1993) *J. Physiol. (London)* **463,** 391–407.
23. Huguenard, J. R. & Prince, D. A. (1994) *J. Neurosci.* **14,** 5485–5502.
24. Golomb, D. & Rinzel, J. (1993) *Phys. Rev. E* **48,** 4810–4814.
25. Golomb, D. & Rinzel, J. (1994) *Physica D* **72,** 259–282.
26. Gloor, P. & Fariello, R. G. (1988) *Trends Neurosci.* **11,** 63–69.
27. Huguenard, J. R. & Prince, D. A. (1994) *J. Neurophysiol.* **71,** 2576–2581.
28. Barkai, E., Kanter, I. & Sompolinsky, H. (1990) *Phys. Rev. A* **41,** 590–597.
29. LoFaro, T., Kopell, N., Marder, E. & Hooper, S. L. (1994) *Neural Comput.* **6,** 69–84.
30. Gray, C. (1994) *J. Comput. Neurosci.* **1,** 11–38.